

Copyright WILEY-VCH Verlag GmbH & Co. KGaA, 69469 Weinheim, Germany, 2016.

ADVANCED OPTICAL MATERIALS

Supporting Information

for *Advanced Optical Materials*, DOI: 10.1002/adom.201600102

Organic Heptamethine Salts for Photovoltaics and Detectors with Near-Infrared Photoresponse up to 1600 nm

*Margaret Young, John Suddard-Bangsund, Tyler J. Patrick,
Natalia Pajares, Christopher J. Traverse, Miles C. Barr,
Sophia Y. Lunt, and Richard R. Lunt**

Supporting Information

Organic Heptamethine Salts for Photovoltaics and Detectors with Near-Infrared Photoresponse up to 1600 nm

By Margaret Young, John D. Suddard-Bangsund, Tyler Patrick, Natalia Pajares, Sophia Y. Lunt, and Richard R. Lunt*

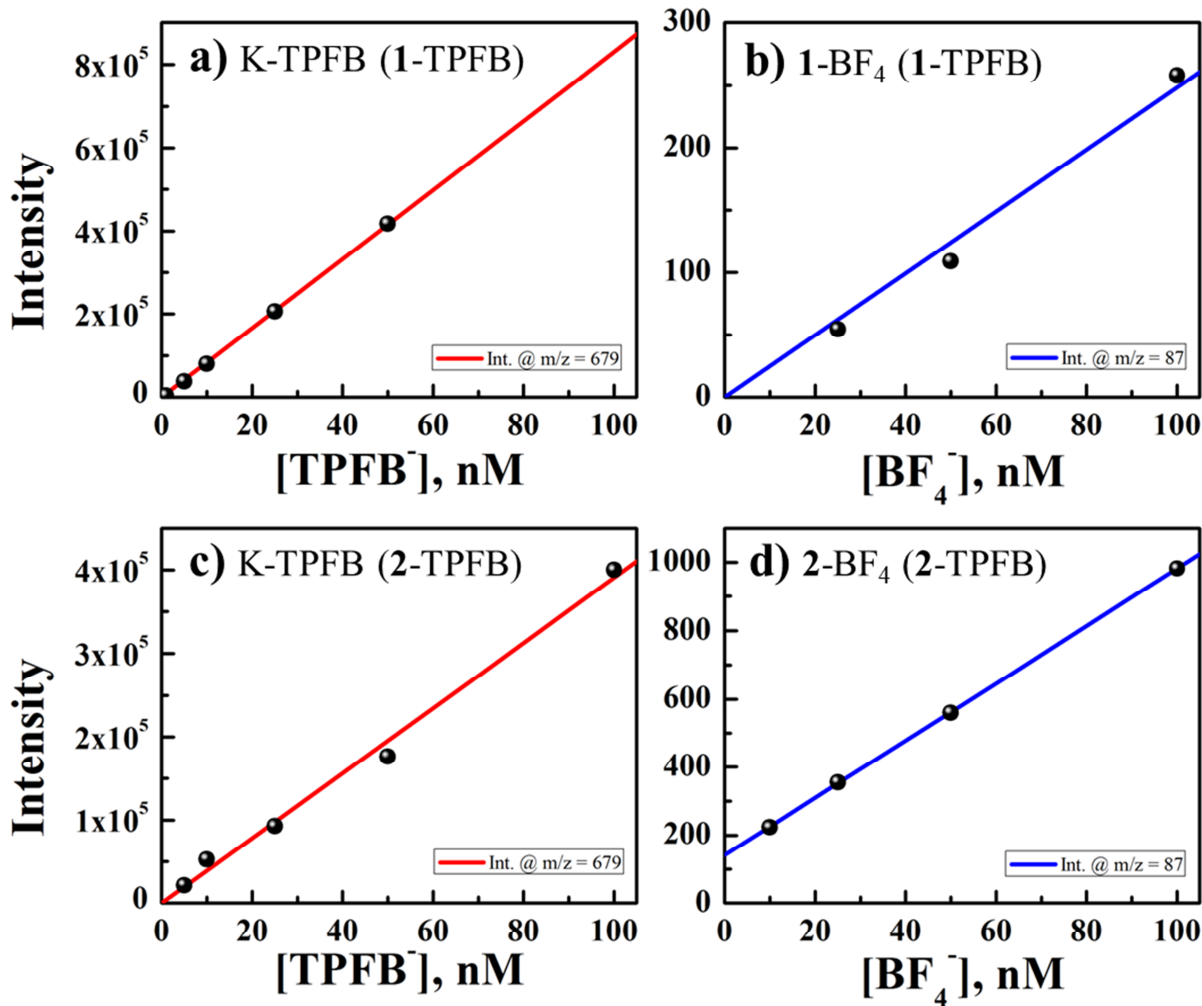
I. Mass Spectrometry Results

Figure S1: (a) Calibration curve of intensity for $m/z = 679$ ($TPFB^-$) signal for K-TPFB standard. (b) Calibration curve for $m/z = 87$ (BF_4^-) for **1**-BF₄ standard. For 100 nM of **1**-TPFB, $[TPFB^-] = 103 \pm 8$ nM and $[BF_4^-]$ was below detectable limits. (c) Calibration curve of intensity for $m/z = 679$ ($TPFB^-$) signal for K-TPFB standard. (d) Calibration curve for $m/z = 87$ (BF_4^-) for **2**-BF₄ standard. For 100 nM of **2**-TPFB, $[TPFB^-] = 110 \pm 5$ nM and $[BF_4^-] = 5 \pm 5$ nM.

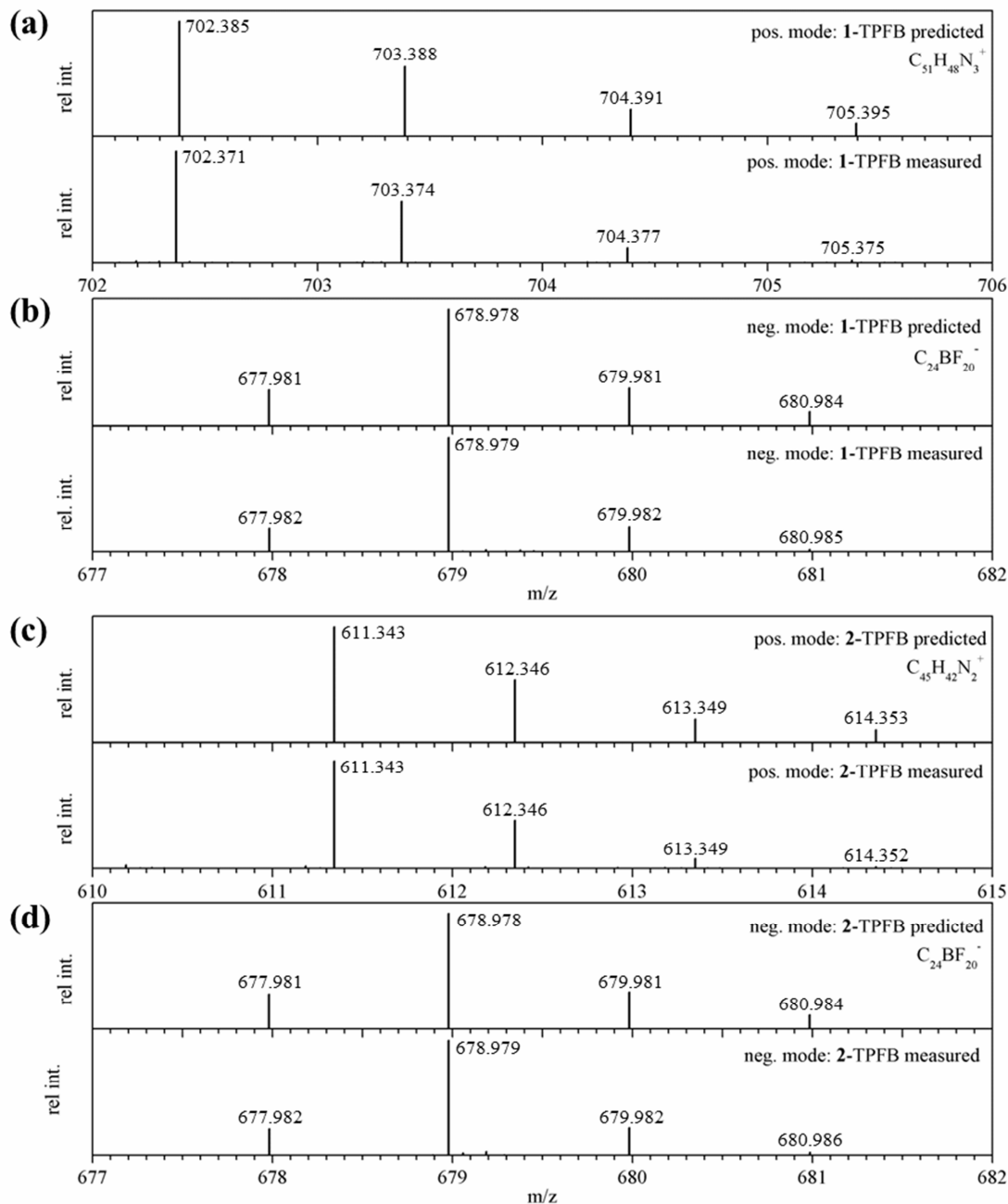


Figure S2: High resolution mass spectrometry verification for **1**-TPFB in (a) positive and (b) negative mode electrospray ionization and for **2**-TPFB in (c) positive and (d) negative mode electrospray ionization. Predicted isotopic abundance peaks for each compound were generated using the Isotope Model tool in MassLynx software.

II. Device Performances

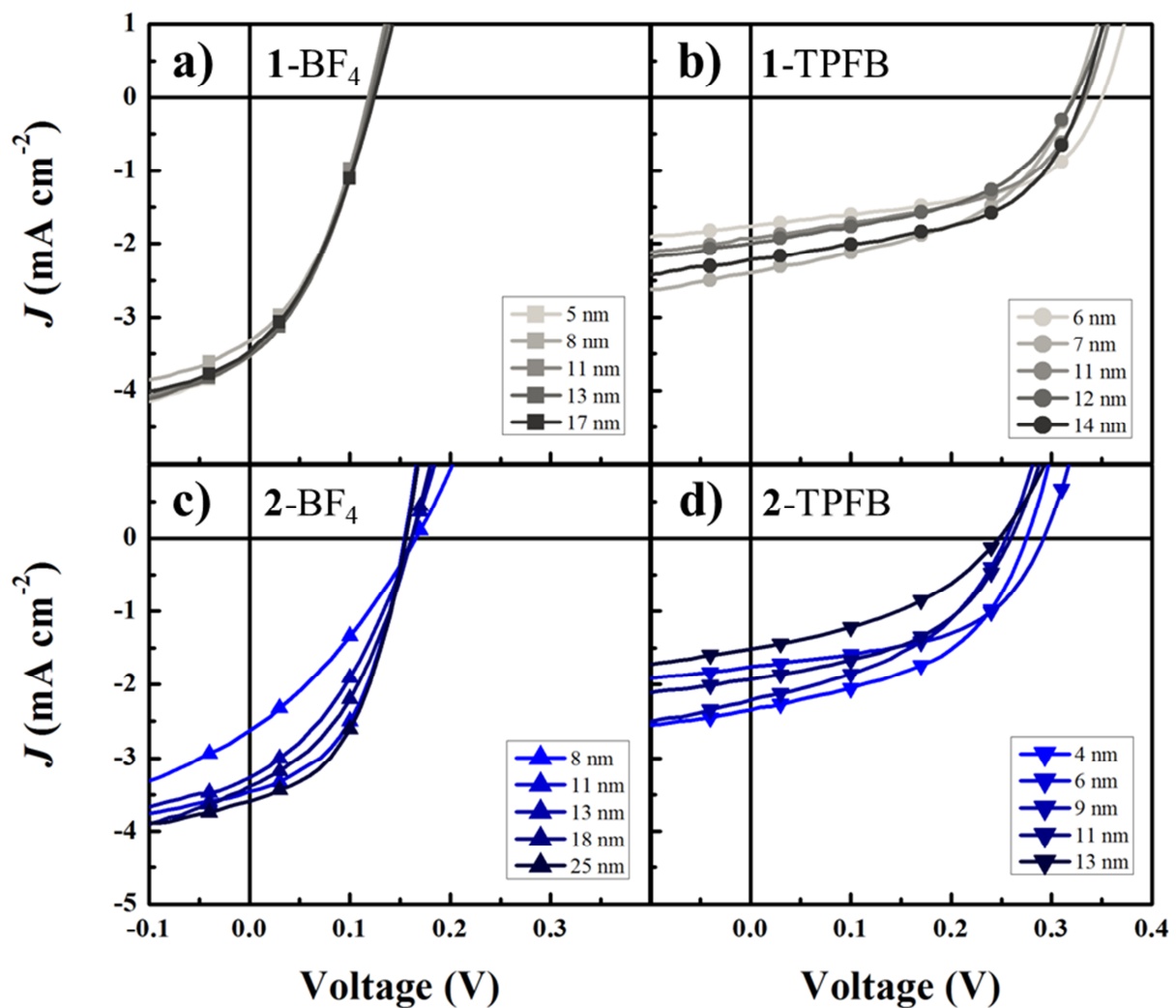


Figure S3: Thickness-dependent 1-sun JV curves for (a) **1-BF₄**, (b) **1-TPFB**, (c) **2-BF₄**, and (d) **2-TPFB**.

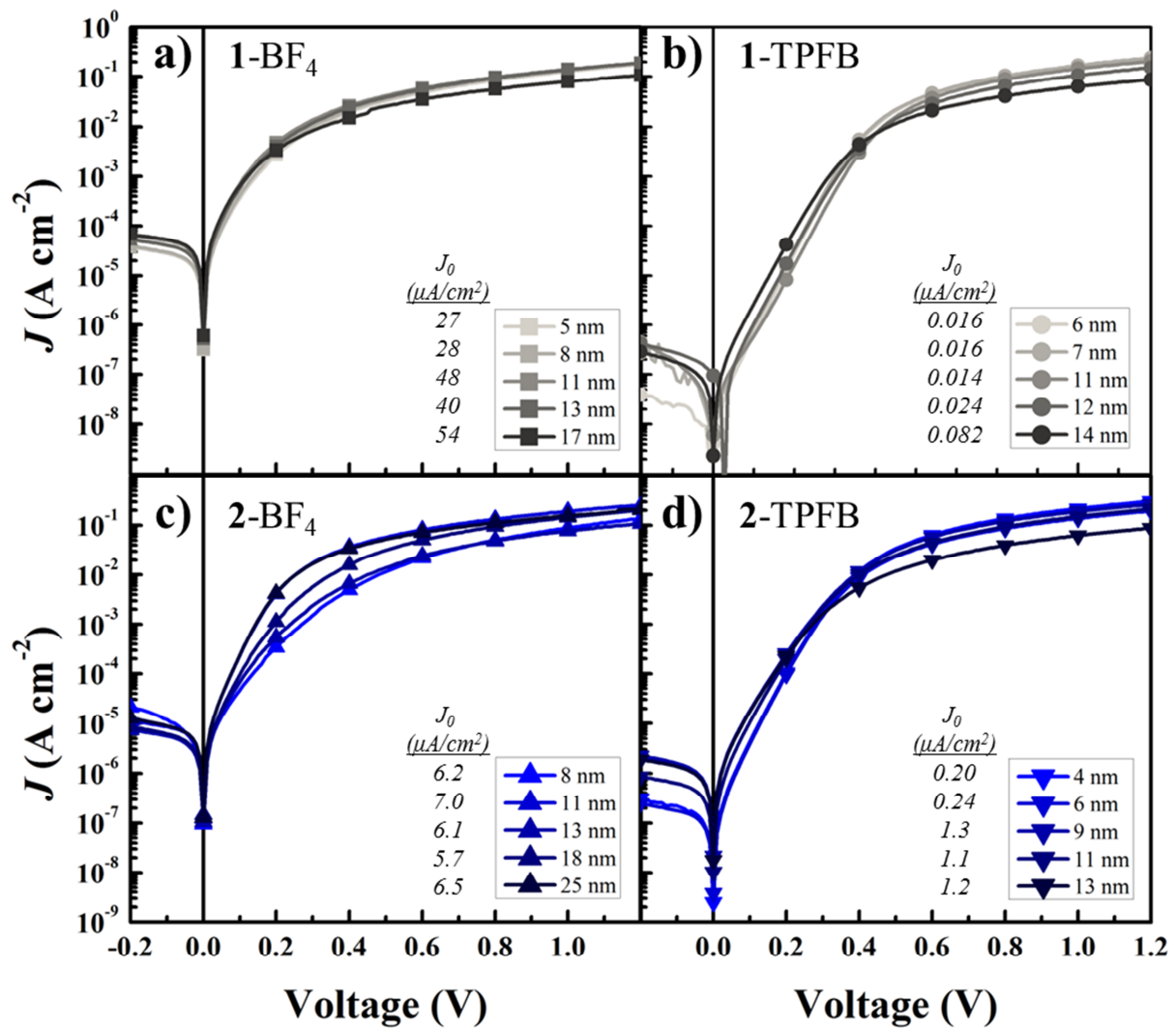


Figure S4: Thickness-dependent dark JV curves for (a) **1-BF₄**, (b) **1-TPFB**, (c) **2-BF₄**, and (d) **2-TPFB**.

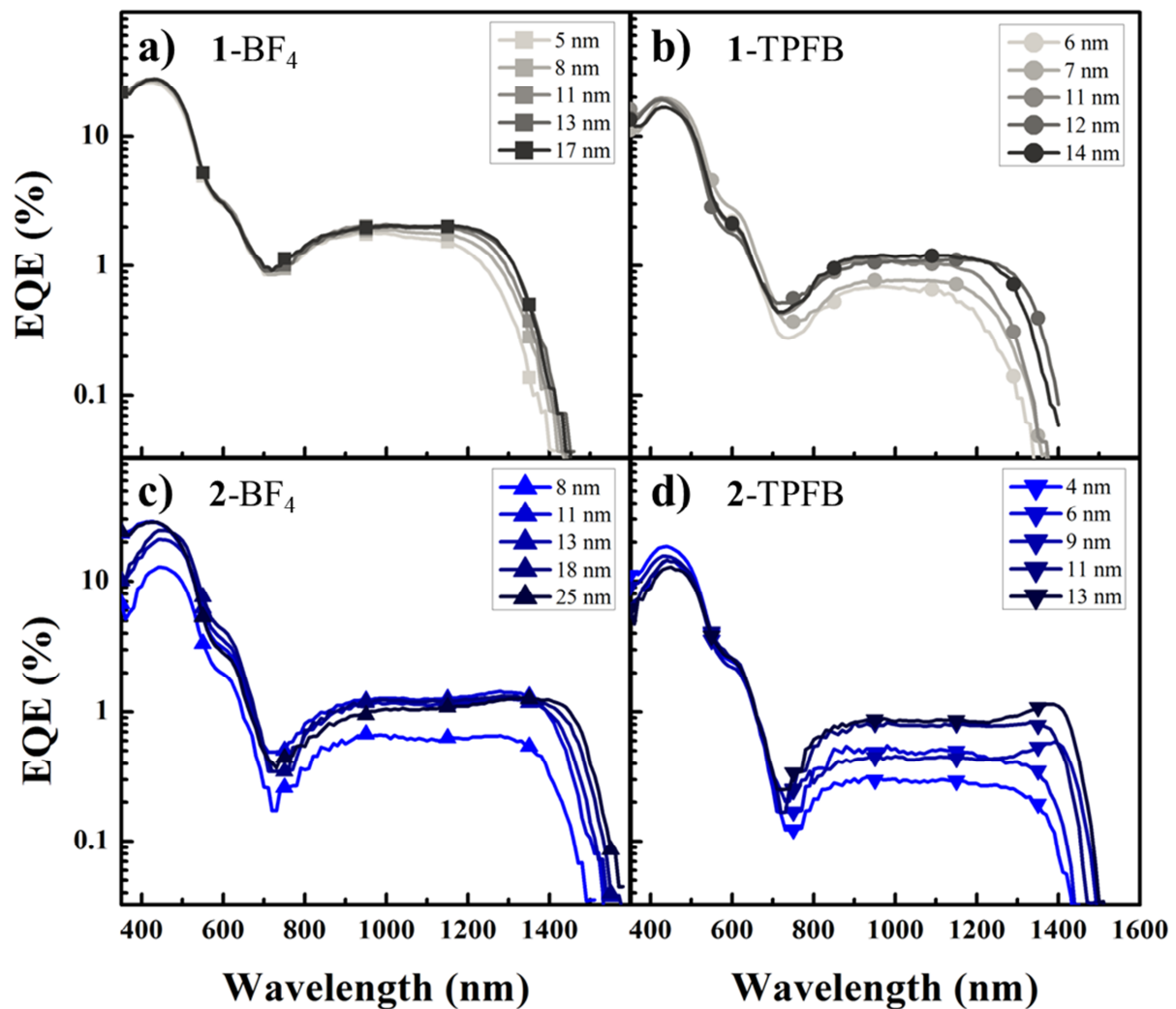


Figure S5: Thickness-dependent EQE curves for (a) **1-BF₄**, (b) **1-TPFB**, (c) **2-BF₄**, and (d) **2-TPFB**.

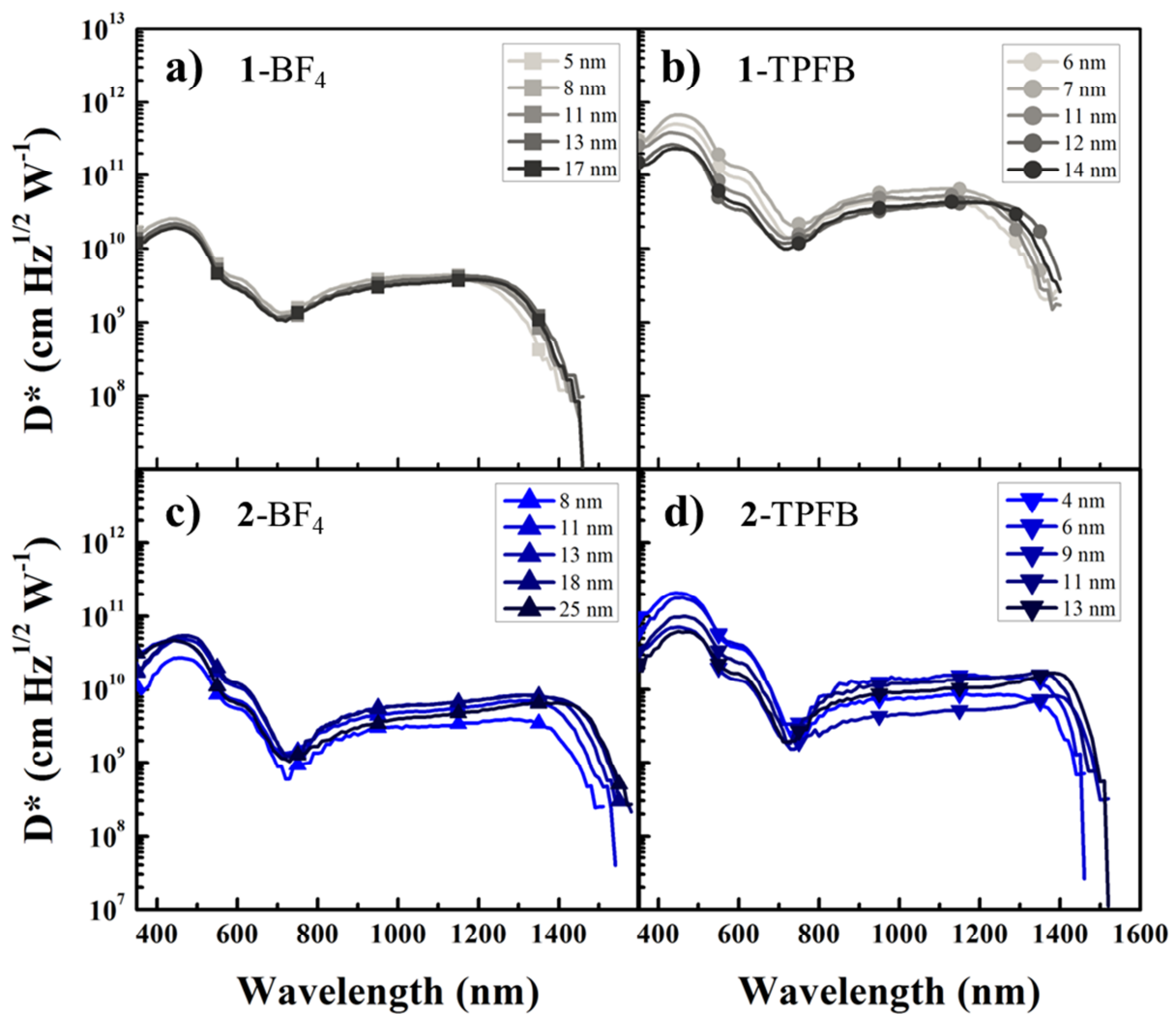


Figure S6: Thickness-dependent detectivity (D^*) curves for (a) **1-BF₄**, (b) **1-TPFB**, (c) **2-BF₄**, and (d) **2-TPFB**.

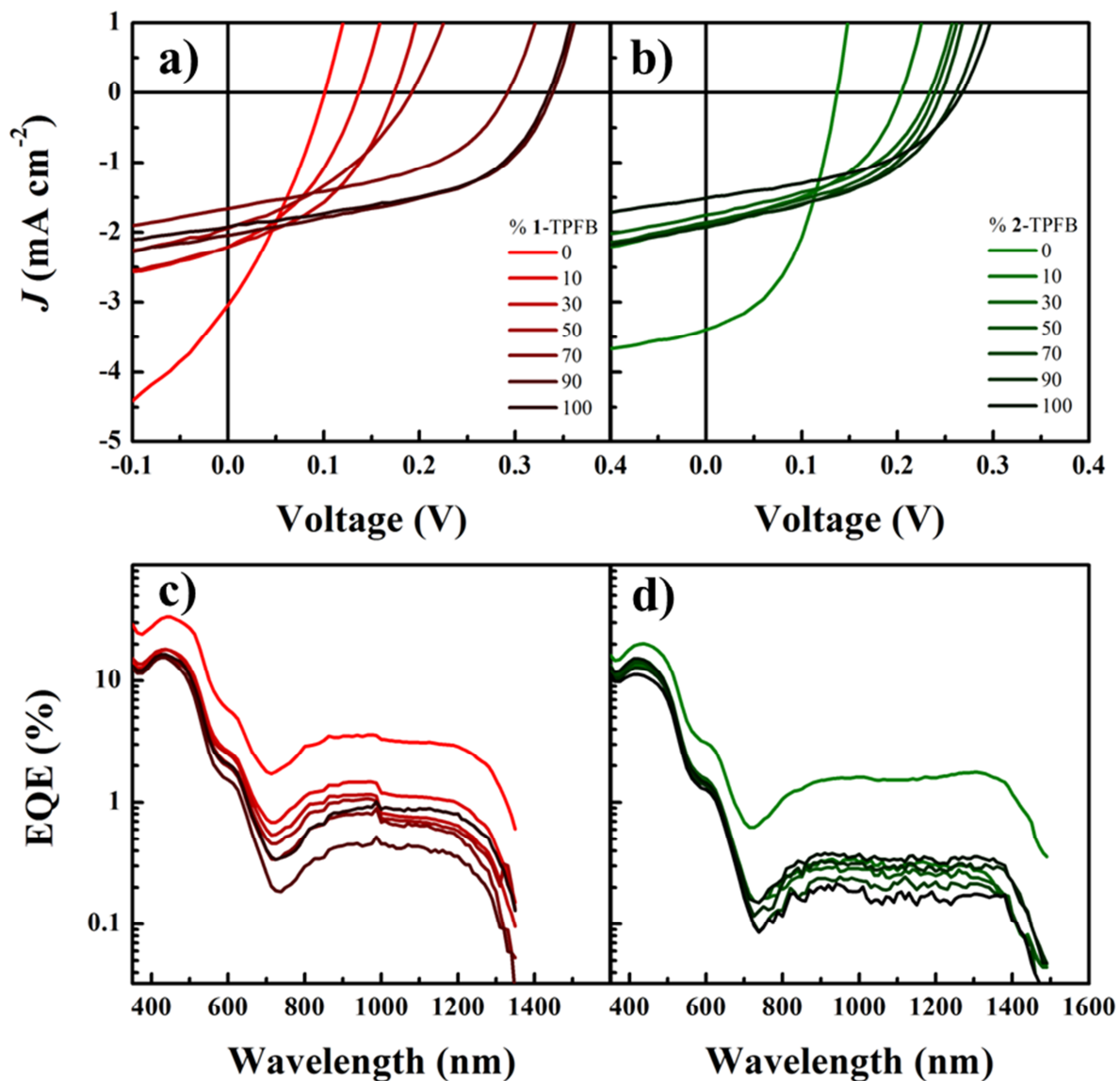


Figure S7: (a) JV curves for as a function of **1**-TPFB molar fraction in a blend of **1**-BF₄ and **1**-TPFB. (b) JV curves as a function of **2**-TPFB molar fraction in a blend of **2**-BF₄ and **2**-TPFB. (c) EQE curves for blended **1** devices, with same legend as in (a). (d) EQE curves for blended **2** devices, with same legend as in (b).

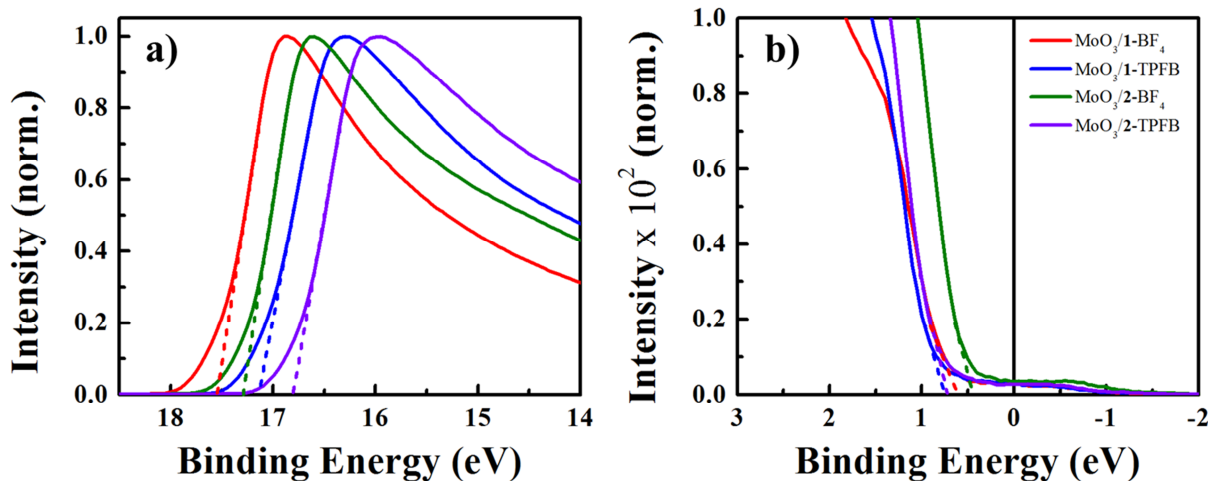


Figure S8: Ultraviolet photoelectron spectroscopy for each salt on ITO / MoO₃. Expanded view of (a) the high energy cutoff and (b) the low energy cutoff.

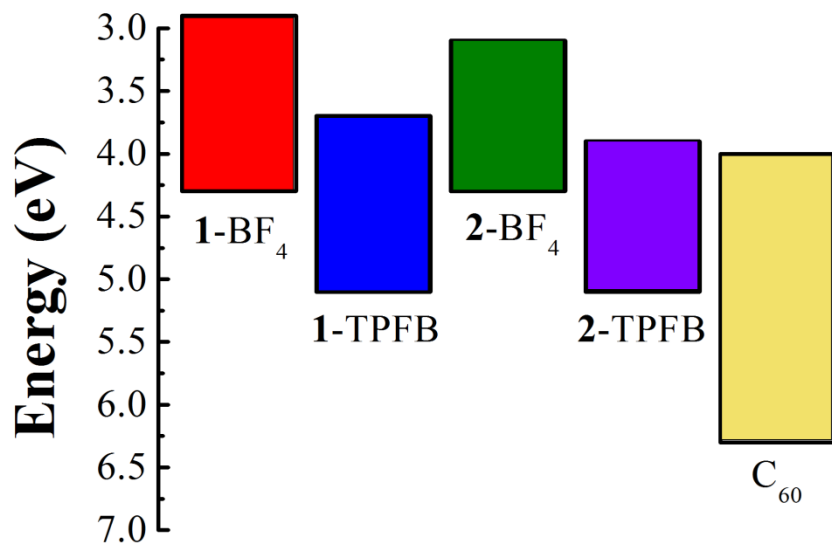


Figure S9: Energy level schematic for each salt measured with UPS and summarized in the table below.

Table S1: Extracted parameters from UPS data: high and low energy cutoffs, work functions and HOMO levels. LUMO levels were estimated by adding the optical bandgap and estimated exciton binding energies to the HOMO level.

Material	High Cutoff (eV)	Low Cutoff (eV)	Work Function (eV)	HOMO (eV)	Optical Bandgap (eV)	LUMO (eV)
1-BF₄	17.5	0.6	3.7	4.3	0.85	2.9
1-TPFB	17.2	0.7	4.0	5.1	0.85	3.7
2-BF₄	17.3	0.4	3.9	4.3	0.80	3.1
2-TPFB	16.8	0.7	4.4	5.1	0.80	3.9